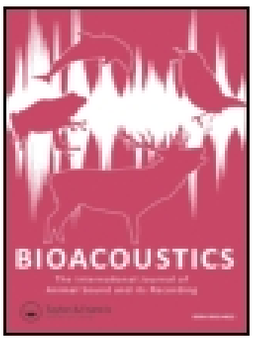

Taylor & Francis
Taylor & Francis Group

Bioacoustics
The International Journal of Animal Sound and its Recording

ISSN: 0952-4622 (Print) 2165-0586 (Online) Journal homepage: http://www.tandfonline.com/loi/tbio20

Modelling the production of complex calls in the túngara frog (Physalaemus pustulosus)

Nicole M. Kime, Michael J. Ryan & Preston S. Wilson

To cite this article: Nicole M. Kime, Michael J. Ryan & Preston S. Wilson (2018): Modelling the production of complex calls in the túngara frog (Physalaemus pustulosus), Bioacoustics, DOI: 10.1080/09524622.2018.1458249

To link to this article: https://doi.org/10.1080/09524622.2018.1458249

Published online: 04 Apr 2018.

BIOACOUSTICS, 2018
https://doi.org/10.1080/09524622.2018.1458249

Taylor & Francis
Taylor & Francis Group

Modelling the production of complex calls in the túngara frog (*Physalaemus pustulosus*)

Nicole M. Kime[a], Michael J. Ryan[b,c] and Preston S. Wilson[d]

[a]Department of Biological Sciences, Edgewood College, Madison, WI, USA; [b]Department of Integrative Biology, University of Texas at Austin, Austin, TX, USA; [c]Smithsonian Tropical Research Institute, Balboa Ancon, Republic of Panama; [d]Department of Mechanical Engineering, University of Texas at Austin, Austin, TX, USA

ABSTRACT

Relatively few studies have used experimental manipulations to investigate the mechanics of vocal production in frogs and toads, even though many frogs produce complex signals with multiple components and/or nonlinearities. Modelling approaches can add to empirical studies by illuminating how various components of the vocal system interact to produce communication signals. In this study, we use bond graphs, a lumped-element modelling technique, to explore how the combination of active modulation of vocal production and the passive dynamics of a unique laryngeal structure result in the complex calls produced by males in an anuran model system. The túngara frog (*Physalaemus* (= *Engystomops*) *pustulosus*) produces advertisement calls with a 'whine' and a facultative 'chuck'. Whines are amplitude and frequency modulated. The chuck is characterized by its spectral complexity and appears to contain a period doubling bifurcation resulting in subharmonics. In our model, we focus on how a fibrous mass attached to the vocal cords results in subharmonics in the chuck. Our models suggest that active (neural) modulation of the fibrous mass is not necessary for the transition between the spectral characteristics of the whine and chuck. Rather, it is possible that the vibratory mode of the fibrous mass and thus the vocal cords changes passively as a result of changes in airflow through the system.

ARTICLE HISTORY
Received 11 January 2018
Accepted 4 March 2018

KEYWORDS
Anuran; túngara frog; advertisement call; fibrous mass; vocal system model; nonlinear

Introduction

Male anurans (frogs and toads) produce advertisement calls with acoustic properties that are decoded by receivers and influence competition for mates (Wilczynski et al. 1995; Gerhardt and Huber 2002; Wells 2007). Even in extensively studied anuran model systems, we know more about how receivers process these calls than about the mechanisms of vocal production (e.g. Wilczynski and Ryan 2010). Relatively few studies have used experimental manipulations to investigate the mechanics of anuran vocal production (Schmidt 1965; Martin 1971; Gans 1973; Gridi-Papp et al. 2006; Suthers et al. 2006; Gridi-Papp 2014; Colafrancesco and Gridi-Papp 2016), and such studies are complicated by the fact that sound production is

CONTACT Nicole M. Kime nkime@edgewood.edu

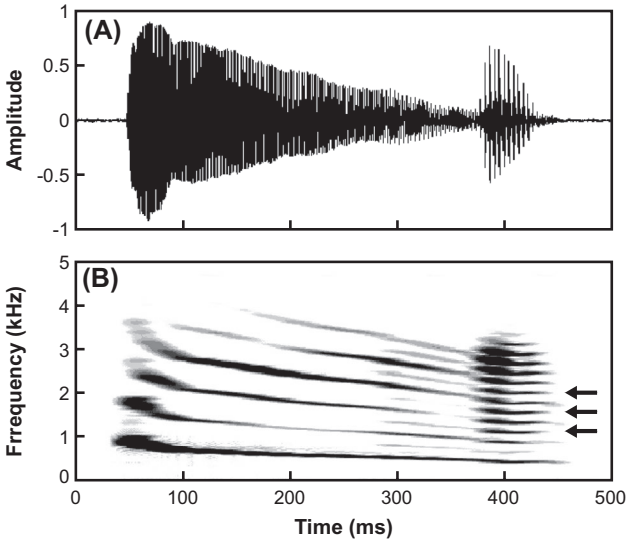

Figure 1. Oscillogram (A) and spectrogram (B) of a túngara frog whine-chuck. Arrows indicate three of the subharmonics in the chuck.

determined by both active (neural) modulation of the vocal system and the passive dynamics of its oscillators. This is particularly true for frogs that produce complex calls. Modelling approaches can add to experimental studies by illuminating how various components of the vocal system interact to produce vocal signals. In a previous study (Kime et al. 2013), we developed a model of the basic anuran larynx. Here, we expand on this work to explore how the combination of active modulation of vocal system components and the passive dynamics of a unique laryngeal structure result in the complex calls produced by males in an anuran model system, the túngara frog (*Physalaemus* (= *Engystomops*) *pustulosus*).

Frogs and toads produce sound when air flow from the lungs to the vocal sac is modulated by the vocal cords. Air from the lungs enters the posterior larynx, where increasing air pressure forces the vocal cords apart. Air flows between the vocal cords at a rate that is dependent on the pressure differential between the two sides of the vocal cords and the area of the opening between them. Pressure in the larynx then decreases, and the elastic vocal cords move back together (Martin 1971; Gans 1973; Kime et al. 2013). The occurrence and frequency of periodic self-sustaining oscillations in the frog vocal system depends on several interacting factors including the rate of air flow into the system, the mass and tension of the vocal cords, additional masses associated with the vocal cords and the behaviour of downstream vocal system elements (Martin 1971; McClelland et al. 1996; Gridi-Papp 2003). In addition, nonlinear phenomena such as subharmonics and frequency jumps have been observed when air flow or pressure changes (Gridi-Papp 2003; Suthers et al. 2006; Feng et al. 2009), or when coupled oscillators interact with each other (Suthers et al. 2006). Across taxa, nonlinear dynamics are common when vocal systems have coupled oscillators and/or are 'driven to their limits' (Fitch et al. 2002).

Male túngara frogs produce an amplitude- and frequency-modulated advertisement call, the 'whine', which may be followed by one or more additional components called 'chucks'

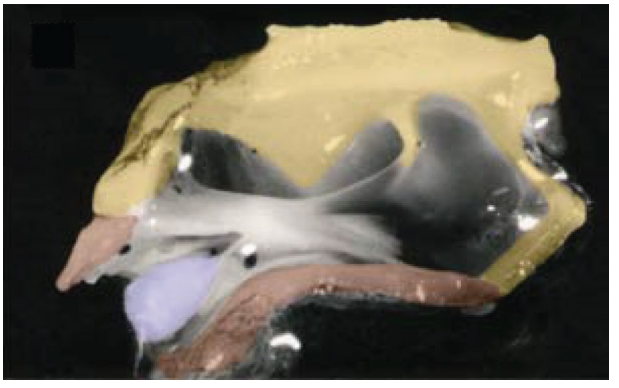

Figure 2. Medial section of a túngara frog larynx showing the vocal cord (white) and attached fibrous mass (blue online). From Gridi-Papp et al. (2006).

(Ryan 1980, 1985; Figure 1(A)). Subharmonics are characteristic of the chuck (Gridi-Papp et al. 2006), and are sometimes also present in whines (Figure 1(B)). The downward frequency sweep of the whine is important for species recognition (Wilczynski et al. 1995). The chuck is favoured by sexual selection; females prefer whines with chucks over whines without chucks (Rand and Ryan 1981) and more chucks to fewer chucks (Akre et al. 2011), especially when chucks contain energy in harmonic frequencies above 1500 Hz (Wilczynski et al. 1995). A chuck with subharmonics is more attractive than a chuck without subharmonics (Ryan et al. 2010; Baugh et al. 2017).

The biomechanics of whine and chuck production in túngara frogs is unresolved. Amplitude modulation in the whine is probably due to changes in air flow from the lungs (Dudley and Rand 1991; Pauly et al. 2006). The whine has a low fundamental frequency for a frog of this size, proposed to be due to the mass of the vocal cords or loading from an additional mass attached to the vocal cords (Drewry et al. 1982; Ryan and Drewes 1990; Gridi-Papp et al. 2006). Frequency modulation of the whine has been proposed to result from decreasing air flow (Dudley and Rand 1991), active changes in the compliance of the vocal cords via changes in the shape of the larynx (Drewry et al. 1982; Ryan and Drewes 1990; Dudley and Rand 1991), and/or changes in air flow combined with vocal cords that act as a hardening spring (Kime et al. 2013).

The production of chucks in túngara frogs and related species is dependent on the presence of a large 'fibrous mass' that is in the route of air flow upstream of the vocal cords (Ryan and Drewes 1990; Boul and Ryan 2004; Gridi-Papp et al. 2006; Baugh et al. 2017) (Figure 2). The fibrous mass is attached to the vocal cords by a thin process that is possibly attached to a transverse thickening of the vocal cords (Drewry et al. 1982; Guerra et al. 2014). Early studies suggested that independent vibration of the fibrous mass when it is facultatively moved into the air flow might cause the chuck to have a fundamental frequency much lower than the whine (Drewry et al. 1982). However, given our current knowledge of the túngara vocal tract, there is no clear mechanism by which males could actively move this structure (Guerra et al. 2014). In addition, the fact that the apparent fundamental frequency of the chuck is always one-half that of the whine suggests that the chuck actually contains subharmonics that are produced when the fibrous mass undergoes an impact oscillation (Bernal et al. 2009).

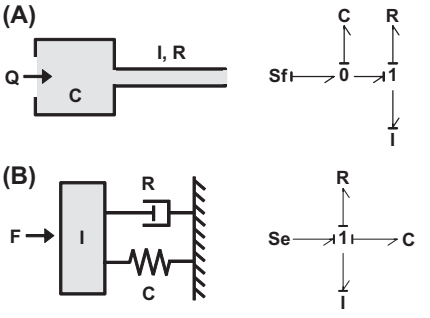

Figure 3. Schematic (left) and bond graph (right) representations of typical vertebrate vocal system components. (A) Air flow into a chamber and then through a narrower tube. (B) Mass-spring damper system representative of a visco-elastic vocal cord. See Table 1 for a description of bond graph elements and examples of how they are used to model the vertebrate vocal system.

In this study, we expand on a previously reported approach to modelling vocal production in frogs (Kime et al. 2013) to investigate the mechanisms by which túngara frogs produce their complex calls. We focus on the role of the fibrous mass in producing the subharmonics of the chuck, and present a lumped-element model of an anuran vocal system in which the passive dynamics of a fibrous mass coupled to the vocal cords causes nonlinearities in its output. We also ask how active modulation of air flow and vocal cord tension might influence the species-specific nonlinear properties of the túngara frog chuck and whine.

Methods and results

We previously described how bond graphs can be used to model vertebrate vocal production systems (Kime et al. 2013; see also Breedveld 2004; Karnopp et al. 2006; Borutzky 2010 for a complete treatment of bond graph methodology). Briefly, bond graphs are lumped-element models of dynamic physical systems. They are domain-independent, which means that they can be used to integrate the pneumatic and mechanical elements of animal vocal production systems. Modelling begins with a bond graph, a graphic representation of the system and power flow among its elements. One can then derive system equations from a causal model, and simulate the behaviour of the system. In this section, we describe these three stages in modelling the production of complex calls in the túngara frog. We used the commercial software program 20-sim (Version 4.1, Controllab Products, B.V.) for all modelling and simulation.

Bond graphs

We translated known anatomical components of the túngara frog larynx, as well as postulated causal interactions among them, into bond graph models. Figure 3 shows examples of two simple bond graphs that describe generalized components of a vertebate vocal system. Each bond graph is comprised of *elements* (represented as letters) connected by *power bonds* through which energy is transferred. Elements are domain-independent and can thus represent pneumatic or mechanical aspects of the vocal system (Table 1). Power bonds show the direction of positive power transfer between elements in the *half-arrow* at one end of

Table 1. Bond graph elements and examples of their application to vertebrate vocal systems.

Element	Type	Examples
Sf	Source of flow	Volume flow rate from lungs
Se	Source of effort	Air pressure
		Muscle force
C	Stores flow	Air volume
		Elastic tissue
I	Stores effort	Fluid in a tube
		Masses
R, MR	Dissipates effort or flow	Friction
		Aperture
		Tissue viscosity
TF	Transformer	Air pressure to mechanical force
0-junction	Distributes flow	Some flow stored in a volume, some exits
1-junction	Distributes effort	Force distributed among a mass, spring, damper

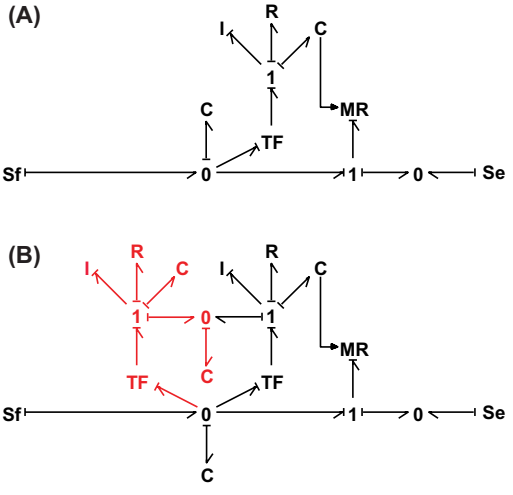

Figure 4. Bond graphs of vocal system models. (A) Control model, a simplified anuran larynx with posterior laryngeal chamber and one vocal cord. (B) Túngara frog model with a fibrous mass coupled to the vocal cord (in red).

the bond. Power is expressed as the product of an effort and a flow; if an effort (e.g. force, or air pressure) is applied to a particular bond graph element then a flow (e.g. velocity, volume flow rate) must be its conjugate output, and vice versa. In Figure 3(A), for example, air flow stored in a volume (C) returns pressure as its output. For each power bond, the element to which effort is applied is indicated by the perpendicular line, or *power stroke*. Kime et al. (2013) describes bond graph modelling of vocal production systems in more detail.

Our control model of frog vocal production is the simple anuran larynx modelled in Kime et al. (2013, Figure 4(A)). This bond graph represents a half-larynx; one lung, one vocal cord, and one-half of the volume of the posterior laryngeal chamber is included. The control model begins with a source of flow (**Sf**) into the larynx from the lungs. At the first 0-junction, some flow is stored in the posterior laryngeal chamber (**C**). This determines pressure in the posterior larynx. Pressure is transformed (**TF**) into a force that displaces the vocal cord. The vocal cord is modelled as a viscoelastic mass-spring-damper system

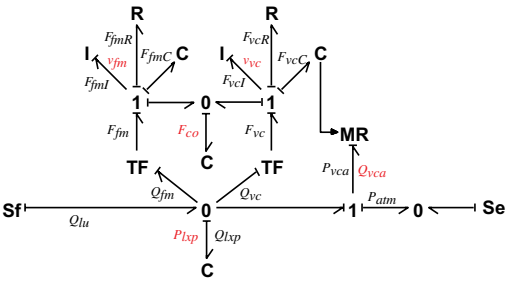

Figure 5. Bond graph of the túngara frog model, including selected efforts (P = pressure, F = force) and flows (Q = volume flow rate, v = velocity) discussed in the text. Subscripts refer to components of túngara frog anatomy, including the lungs (*lu*), posterior laryngeal chamber (*lxp*), vocal cord (*vc*), fibrous mass (*fm*), and vocal cord aperture (*vca*). At 0-junctions, efforts are equal and determined by only one of the bonds (highlighted in red). At 1-junctions, flows are equal and determined by only one of the bonds (highlighted in red).

(**I**, **C**, **R**, respectively). The rate of air flow through the vocal cord aperture (**MR**) is determined by the displacement of the vocal cord and pressure in the posterior laryngeal chamber. In this model, pressure downstream of the vocal cord is simply a reference atmospheric pressure (**Se** = 0).

To model the túngara frog's fibrous mass, we added a second mass-spring-damper system (**I, C, R**) to the control model (Figure 4(B)). This structure is coupled to the vocal cord with an elastic 'spring' (**C**) that represents the process connecting the fibrous mass and vocal cord (e.g. Figure 2, Drewry et al. 1982; Guerra et al. 2014). The direction of the half-arrows and power stroke show that both the fibrous mass and the vocal cord transfer energy to this coupling and that, when displaced, the elastic coupling applies force to both the vocal cord and fibrous mass. This simplified two-dimensional model assumes that pressure in the posterior larynx moves the vocal cord and the fibrous mass in different directions, thus stretching the elastic tissue that connects them.

System equations

We used the modelling software 20-sim (Version 4.1, Controllab Products, B.V.) to derive system equations. These equations are valid for lumped element models in which the wavelength of sound produced is much larger than the size of individual vocal system components (Fletcher 1992); this is true for túngara frogs, which have a body size of ~30 mm and produce calls with fundamental frequencies less than 1000 Hz (>300 mm wavelength). System equations for the control model are described in Kime et al. (2013). We summarize equations for the fibrous mass model below. Figure 5 shows selected effort and flow variables mapped onto the fibrous mass bond graph model.

A first set of equations describes the relationship between air flow and pressure in the posterior larynx. The model begins with a source of flow (**Sf**) into the larynx from the lungs. The volume flow rate into the system from one lung is Q_{lu}. This flow is partitioned at the first **0-junction** such that some flow is stored in the posterior laryngeal chamber, some passes through the vocal cord aperture, and some is transformed to the velocity of the vocal cord and fibrous mass:

$$Q_{lu} = Q_{lxp} + Q_{vca} + Q_{vc} + Q_{fm}. \tag{1}$$

Flow is stored in the fluid capacitance of the posterior laryngeal chamber (**C**), at a rate equal to Q_{lxp}. The displacement of air in the posterior laryngeal chamber is the integral of this stored flow over time:

$$X_{lxp} = \int^t Q_{lxp}\, dt. \tag{2}$$

The compliance (compressibility) of this air volume is determined by the standard equation:

$$C_{lxp} = \frac{V_{lxp}}{\rho c^2}, \tag{3}$$

where V_{lxp} is the volume of the chamber, ρ is the density of air, and c is the speed of sound in air (Fletcher 1992; Karnopp et al. 2006). Pressure, which is determined by the displacement of air and the compliance of the air volume, is the conjugate output of flow stored in the posterior laryngeal chamber:

$$P_{lxp} = \frac{X_{lxp}}{C_{lxp}}. \tag{4}$$

Pressure in the posterior laryngeal chamber determines effort at the first 0-junction. At the two transformers (**TF**), pressure is transduced to a force that can displace the vocal cord (*vc*) and the fibrous mass (*fm*) from their resting positions. The magnitude of this force also depends on the area (*A*) of each structure against which air presses:

$$F_{vc} = P_{lxp} * A_{vc}. \tag{5}$$

$$F_{fm} = P_{lxp} * A_{fm}. \tag{6}$$

Two parallel sets of equations then describe the movement of the vocal cord (*vc*) and the fibrous mass (*fm*). The vocal cord and the fibrous mass are modelled as two mass-spring-damper systems (**I**, **C**, **R** elements, respectively) coupled together by an elastic spring (**C**). At the **1-junctions**, the force applied to each structure is partitioned among these elements. Part of the force is applied to the mass (**I**) of each structure:

$$F_{vcI} = F_{vc} - F_{vcC} - F_{vcR} - F_{co}. \tag{7}$$

$$F_{fmI} = F_{fm} - F_{fmC} - F_{fmR} - F_{co}. \tag{8}$$

Momentum (*p*) is the integral of force applied to the mass of the vocal cord or fibrous mass over time:

$$p_{vc} = \int^t F_{vcI} dt. \tag{9}$$

$$p_{fm} = \int^t F_{fmI} dt. \tag{10}$$

The velocity of the vocal cord or fibrous mass depends on their momentum and mass (m):

$$v_{vc}=\frac{p_{vc}}{m_{vc}}. \tag{11}$$

$$v_{fm}=\frac{p_{fm}}{m_{fm}}. \tag{12}$$

The velocity of the vocal cord and fibrous mass determine the behaviour of the **C** (spring) and **R** (damper) elements of the model. The displacement (X) of the elastic tissue (**C**) associated with the vocal cord and the fibrous mass is the integral of their velocity. At any given time,

$$X_{vc} = \int^t v_{vc} dt. \tag{13}$$

$$X_{fm} = \int^t v_{fm} dt. \tag{14}$$

By Hooke's law, a displaced spring provides a restoring force proportional to its displacement and compliance. For a linear spring, the restoring force is:

$$F_{vcC} = \frac{X_{vc}}{C_{vc}}. \tag{15}$$

$$F_{fmC} = \frac{X_{fm}}{C_{fm}}. \tag{16}$$

where C_{vc} and C_{fm} are the compliance of the vocal cord and fibrous mass tissues in their range of free movement. If the vocal cord or the fibrous mass collides with something, further displacement is restricted and impact oscillations can occur. This is modelled as additional restoring forces at the resting position of the vocal cord and fibrous mass and at the lateral margin of the larynx (Ishizaka and Flanagan 1972; Story and Titze 1995). When the vocal cord or fibrous mass reaches these locations, the restoring force changes to:

$$F_{vcC} = \frac{X_{vc}}{C_{vc}} + \frac{X_{vc}}{C_{vc2}}. \tag{17}$$

$$F_{fmC} = \frac{X_{fm}}{C_{fm}} + \frac{X_{fm}}{C_{fm2}}. \tag{18}$$

where C_{vc2} and C_{fm2} represent reduced compliance of the vocal cord and fibrous mass when movement is restricted. In Equations (7) and (8), this restoring force opposes the force applied to the vocal cord and fibrous mass from air pressure in the posterior larynx.

Some of the force applied to the vocal cord and the fibrous mass is dissipated by the viscous properties of the tissue (**R**). The amount of force dissipated from the system depends on the damping coefficient and the velocity of each structure:

$$F_{vcR} = b_{vc} v_{vc}. \tag{19}$$

$$F_{fmR} = b_{fm} v_{fm}. \tag{20}$$

where b is the damping coefficient, which is determined by the standard equation:

$$b_{vc} = 2\zeta_{vc} \sqrt{\frac{m_{vc}}{C_{vc}}}. \tag{21}$$

$$b_{fm} = 2\zeta_{fm} \sqrt{\frac{m_{fm}}{C_{fm}}}. \tag{22}$$

in which zeta is the damping ratio (Karnopp et al. 2006).

The coupling between the vocal cord and the fibrous mass is modelled as a third spring (**C**). At the **0-junction**, the velocity of this spring (how fast the link between the FM and the VC is stretching) is determined by the velocity of the fibrous mass and the velocity of the vocal cord:

$$v_{co} = v_{vc} + v_{fm}. \tag{23}$$

The displacement of the coupling spring is then the integral of its velocity over time:

$$X_{co} = \int^t v_{co} dt. \tag{24}$$

By Hooke's law, the restoring force of the coupling spring is its displacement divided by its compliance. In this model,

$$F_{co} = \frac{\mathrm{X}_{co}}{C_{co}}. \tag{25}$$

where C_{co} is the compliance of the tissue connecting the vocal cord and fibrous mass. In Equations (7) and (8), this restoring force opposes the force applied to the vocal cord and fibrous mass from air pressure in the posterior larynx.

One additional aspect of the system that is influenced by the velocity of the vocal cord and fibrous mass is the volume flow rate at the transformer. This is the amount of flow from the lungs that is transformed to the movement of each structure in Equation (1).

$$Q_{vc} = v_{vc} * A_{vc}. \tag{26}$$

$$Q_{fm} = v_{fm} * A_{fm}. \tag{27}$$

A final equation describes the flow of air through the vocal cord aperture. The rate of flow depends on how much the vocal cord is displaced, as well as the difference between pressure in the posterior laryngeal chamber and pressure anterior to the vocal cord (**Se**). It does not depend on the displacement of the fibrous mass. We used a nonlinear equation for the rate of flow through an orifice (Ishizaka and Flanagan 1972; Karnopp et al. 2006; Riede et al. 2011):

$$Q_{vca} = C_d A_{vca} \sqrt{\frac{2|P_{vca}|}{\rho}} \mathrm{sgn} P_{vca}. \tag{28}$$

In this equation, the constant C_d is the discharge coefficient for flow through an aperture, and the constant ρ is the density of air. A_{vca} is the area of the vocal cord aperture, which is modelled as an ellipse with one fixed axis and one axis determined by the displacement of the vocal cord. The area of the vocal cord aperture is bounded at zero and increases with vocal cord displacement. P_{vca} is the pressure difference between the posterior laryngeal chamber and a reference pressure (**Se** = 0) in the supra-laryngeal environment, and $\mathrm{sgn} P_{vca}$ is the sign of this pressure difference.

In summary, this model expands upon the anuran larynx model presented in Kime et al. (2013) to include a fibrous mass coupled to the vocal cord. Pressure in the posterior laryngeal chamber is transformed to a force that acts on the vocal cord and fibrous mass (Equations (1)–(6)). Because the velocity of these structures depends on parameters such as area, mass, and tissue compliance, they may have very different displacements (Equations (7)–(22)). In this model, elastic tissue coupling the vocal cord and fibrous mass adds a restoring force (Equations (23)–(25)) that modifies the movement of each structure. A large restoring force limits the displacement of the vocal cord (Equation (7)). This in turn influences the rate of flow through the vocal cord aperture (Equation (28)).

Model simulation

We simulated models in the software program 20-sim (Controllab Products, B.V.). We compared the control (Figure 4(A)) and fibrous mass (Figure 4(B)) models to investigate how coupling a fibrous mass to the vocal cord might influence the dynamics of vocal cord oscillation and thus nonlinearities in vocal production. Simulation parameters (Table 2) were estimated from published information on túngara frogs or other vertebrates (Dudley and Rand 1991; Story and Titze 1995; McClelland et al. 1996; Boul and Ryan 2004; Riede et al. 2011; Guerra et al. 2014); not all of the parameters have been systematically measured for túngara frogs. In initial simulations of the control and fibrous mass models and in the sensitivity analyses described below, all model parameters were kept constant over the time course of the simulation.

Túngara frogs may actively modulate air flow and vocal cord compliance when producing amplitude and frequency modulated whines and chucks (Drewry et al. 1982; Dudley and Rand 1991; see also Martin 1971; Gridi-Papp 2014). In two additional 'whine-chuck' simulations, we concurrently modulated air flow and vocal cord compliance over the course

Table 2. Parameters and constants for model simulations.

Parameter or Constant		Model	
		Control	Fibrous Mass
Q_{lu}	Flow rate from one lung[a,*]	3×10^{-6} m^3/s	
V_{lxp}	Posterior larynx volume (half)[b]	6×10^{-8} m^3	
r_{lx}	Larynx radius[b]	3×10^{-3} m	
A_{vc}	Vocal cord (VC) effective area[b,c]	2×10^{-6} m^2	
m_{vc}	VC mass[d]	3×10^{-7} kg	
C_{vc}	VC compliance[e,*]	0.2 m/N	
C_{vc2}	VC compliance at larynx median[e]	1×10^{-5} m/N	
ζ_{vc}	VC damping ratio[e]	0.1	
C_{co}	Compliance of VC – FM coupling[e]	–	0.6 m/N
A_{fm}	Fibrous mass (FM) effective area[b]	–	2×10^{-6} m^2
m_{fm}	FM mass[c]	–	7×10^{-7} kg
C_{fm}	FM compliance[e]	–	0.2 m/N
C_{fm2}	FM compliance at median[e]	–	1×10^{-5} m/N
ζ_{fm}	FM damping ratio[e]	–	0.1
ρ	Density of air[f]	1.21 kg/m^3	
c	Speed of sound in air[f]	343 m/s	
C_d	Discharge coefficient through orifice[f]	0.62	

Notes: Parameters estimated from: (a) Dudley and Rand (1991); (b) Boul and Ryan (2004); (c) Guerra et al. (2014), Guerra (personal communication); (d) McCelland et al. (1996); (e) not available for anurans or túngara frogs, see text and Kime et al.(2013); (f) Karnopp et al. (2006).

For the fibrous mass model, only differences from the control model are included. Two additional 'whine-chuck' simulations added modulation of air flow from the lungs and vocal cord compliance to the control and fibrous mass models. Flow decreased exponentially from 5×10^{-6} m^3/s to 1×10^{-6} m^3/s over 350 ms (whine) and then increased to 5×10^{-6} m^3/s for an additional 60 ms (chuck). In addition, compliance of the vocal cord increased from 0.1 to 0.2 m/N over 350 ms (whine) and then remained at 0.2 m/N for an additional 60 ms (chuck).

of the simulation in order to 'mimic' túngara frog vocal behaviour. As above, one model included a fibrous mass while a control model did not. For both models, air flow from the lungs ($\mathbf{Q_{lu}}$ in Figure 5) decreased exponentially over the first 350 ms of the simulation (the duration of a typical whine) and then increased again for 60 ms (the chuck). Compliance of the vocal cord ($\mathbf{F_{vcC}}$ in Figure 5) also increased linearly for 350 ms (whine) and then remained constant for the subsequent 60 ms (chuck) (Table 2).

We used 20-sim's variable time-step Backward Differentiation Formula as the integration method with absolute and relative tolerances of 1.0×10^{-15}. Quantitative output variables included pressure in the posterior laryngeal chamber, displacement of the fibrous mass, displacement of the vocal cord, and volume flow rate through the vocal cord aperture as a function of time. We evaluated these output variables for the following characteristics. First, we considered a simulated model to be a sound source if it had persistent self-sustaining oscillations in vocal cord displacement and flow through the larynx for the duration of the simulation. This is predicted for successful models but not inevitable for all combinations of parameters. We used Fast Fourier Transform (FFT) analysis to calculate the frequency content of these oscillations. We compared this to the typical fundamental frequency of túngara frog calls as a second indicator of success. We also compared frequency between fibrous mass and control models.

We visually inspected plots of output variables for nonlinearities in the displacement of the vocal cord and fibrous mass, specifically period doubling, impact nonlinearities, and bifurcations (sensu Wilden et al. 1998). For the purposes of this paper, we define period doubling as a circumstance in which the modelled vocal cord completed two or more cycles of displacement before repeating its pattern of motion. Impact nonlinearities occur

when oscillators collide with another structure (such as collision of the two vocal cords at the median of the larynx). For 'whine-chuck' simulations with varying parameters, we also noted the presence of bifurcations, or sudden changes in the dynamics of vocal cord displacement with continuously varying parameters.

In túngara frogs, vocal system anatomy and vocal behaviour vary extensively within and among individuals. For example, individuals modulate air flow from the lungs and perhaps vocal cord compliance within calls (Drewry et al. 1982; Dudley and Rand 1991). The rate of air flow from the lungs also varies among calling bouts (Pauly et al. 2006). The morphology of the vocal cords and the fibrous mass changes as male frogs develop to maturity (Guerra et al. 2014). To investigate the sensitivity of our models to input parameters, we simulated the fibrous mass model with parameters that systematically varied from the values listed in Table 2. We report data from 324 additional simulations in which we varied the size of the fibrous mass, tissue compliance, and/or air flow between 50 and 150% of our estimated system parameters. Given available information (e.g. Boul and Ryan 2004; Guerra et al. 2014), we assume that this encompasses variation in the morphology and behaviour of adult (calling) male túngara frogs. We visually inspected the output of each of these simulations for the presence of self-sustaining oscillations and for period doubling in the displacement of the vocal cord.

Control and fibrous mass models

Simulation of the control model results in sustained oscillations of the vocal cords at a frequency of 1145 Hz, which is near the fundamental frequency at the beginning of the túngara frog whine (Figure 6 (A)–(C); see also Kime et al. 2013). Pressure in the posterior laryngeal chamber increases with air flow from the lungs when the vocal cords are closed (displacement = 0). This pressure is transduced to a force applied to the vocal cord, which causes them to be displaced from their resting position. Air flows through the vocal cord aperture when the vocal cord are displaced and pressure in the posterior larynx is higher than downstream pressure. Pressure in the posterior laryngeal chamber then decreases. The momentum of the vocal cords causes them to continue positive displacement even after pressure decreases, but they eventually reverse direction because of the restoring force of vocal cord elasticity. The vocal cords thus close with a delay determined by their mass. If the vocal cords collide at the median of the larynx, the impact creates additional force displacing the vocal cords from their resting position in their next cycle of oscillation.

Adding a fibrous mass coupled to the vocal cords changes the dynamics of vocal cord oscillation and results in period doubling (Figure 6 (D)–(F)). In the fibrous mass model, pressure in the posterior laryngeal chamber and impact oscillations cause displacement of both the vocal cords and the fibrous mass from their resting positions (displacement = 0). Both structures reverse direction because of the restoring forces of tissue elasticity, which in this model includes the additional restoring force of the coupling between the vocal cords and fibrous mass. The coupling between the vocal cords and fibrous mass has important implications for their oscillation dynamics. The movement of the fibrous mass is tied to pressure in the posterior larynx, which is ultimately determined by the opening and closing of the vocal cords. The frequency of oscillation of the fibrous mass is thus entrained to the frequency of vocal cord oscillation. The larger fibrous mass does not, however, return to its initial position or experience an impact oscillation with every oscillation of the vocal cords. Because the restoring force applied to the vocal cord depends in part on the displacement

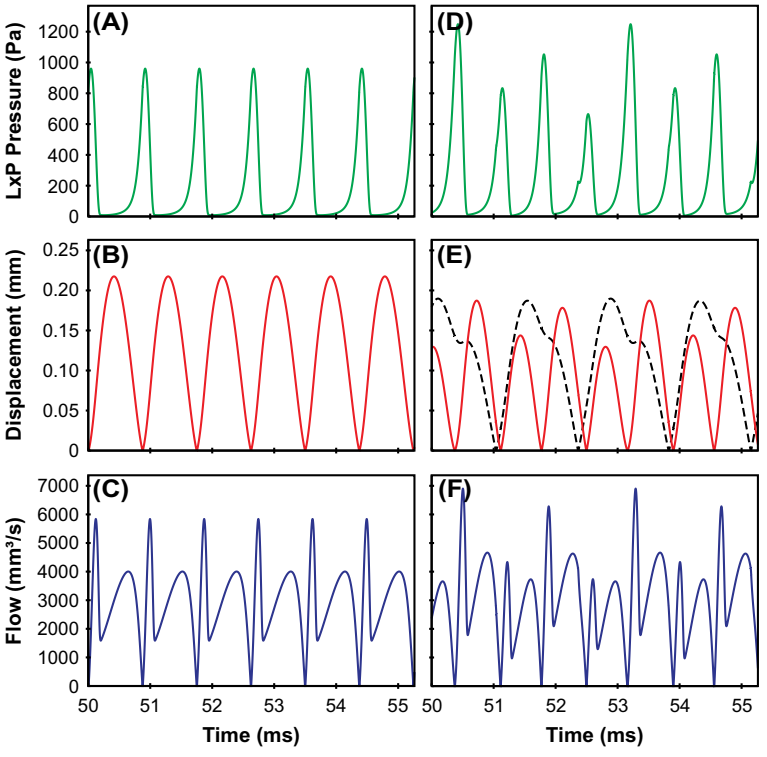

Figure 6. Output for the control (A–C) and fibrous mass (D–F) models, showing 5 ms of sustained oscillations from each model. Simulation parameters are listed in Table 2. Output variables are pressure in the posterior larynx (A and D, green), displacement of the vocal cord (B and E, red), displacement of the fibrous mass (E, black dotted) and flow through the vocal cord aperture (C and F, blue).

of the fibrous mass, this results in period doubling in vocal cord oscillation. In addition, the vocal cords have less overall displacement because of the restoring force of the coupling between the vocal cords and the fibrous mass. The fundamental frequency of the vocal cords therefore increases to 1435 Hz in the fibrous mass model. In summary, a large fibrous mass coupled to the vocal cords modulates their displacement and airflow between them, resulting in period doubling in vocal cord oscillation.

Period doubling in the fibrous mass model is evident over a range of parameter values in which the fibrous mass undergoes impact oscillation and (via its coupling) provides a restoring force to the vocal cords that is sufficient to modify their mode of oscillation (Figures 7 and 8). The restoring force supplied by the fibrous mass to the vocal cords depends on its displacement and the compliance of its coupling to the vocal cords. A larger fibrous mass has greater displacement and experiences impact oscillations (Figure 7(A) and (B)). Period doubling only occurs above a threshold rate of air flow from the lungs, especially for smaller fibrous masses (Figure 8(A)). Likewise, when the fibrous mass is small, a restoring force sufficient to result in period doubling requires lower compliance of the vocal cords (Figure 8(B)), higher compliance of the fibrous mass (which enables it to have greater displacement) (Figure 8(C)), and/or low compliance of the coupling (Figure 7(D) and (E), Figure 8(D)).

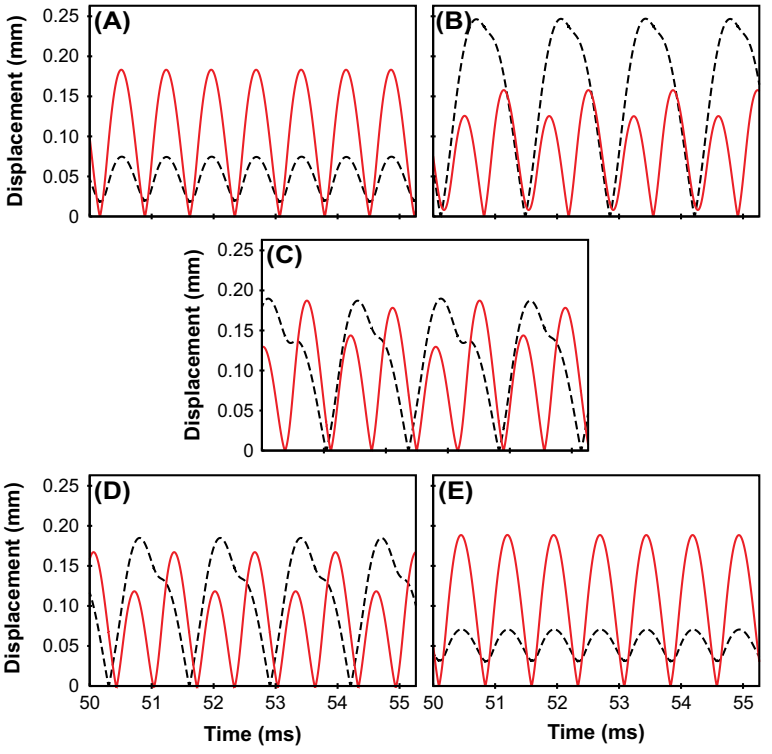

Figure 7. Influence of fibrous mass size (A, B) and coupling compliance (D, E) on the presence of period doubling in vocal cord oscillations. Black dotted lines = fibrous mass displacement, red solid lines = vocal cord displacement. The centre figure (C) includes model parameters as in Table 2: fibrous mass = 7.0×10^{-7} kg, coupling compliance = 0.6 m/N. (A) Small fibrous mass = 5.25×10^{-7} kg, (B) Large fibrous mass = 8.87×10^{-7} kg. (D) Low coupling compliance = 0.45 m/N, (E) High coupling compliance = 0.75 m/N.

Whine-chuck simulations

In the 'whine-chuck' simulations, we concurrently modulated flow from the lungs and vocal cord compliance in order to 'mimic' a túngara frog call. Air flow from the lungs decreased exponentially over the first 350 ms of the simulation (the duration of a typical whine) and then increased again for 60 ms (the chuck). Compliance of the vocal cord increased linearly for a 350 ms 'whine', and then remained constant for a subsequent 60 ms 'chuck'. With these input parameters, the fibrous mass model exhibits period doubling in the chuck but not the whine (Figure 9(B)). A control model without a fibrous mass does not exhibit period doubling in either the whine or the chuck (Figure 9(A)).

Discussion

The túngara frog and some other species within the genus *Engystomops* (= *Physalaemus*) produce complex calls with two distinct components, a 'whine' plus a facultative 'chuck' (Rand and Ryan 1981; Ryan 1985; Boul and Ryan 2004; Gridi-Papp et al. 2006; Bernal et al. 2009; Ryan et al. 2010). Chucks are characterized by subharmonics, spectral components that are an integer fraction of the fundamental frequency. The production of complex calls, and especially the subharmonics of the chuck, is associated with a large fibrous mass attached

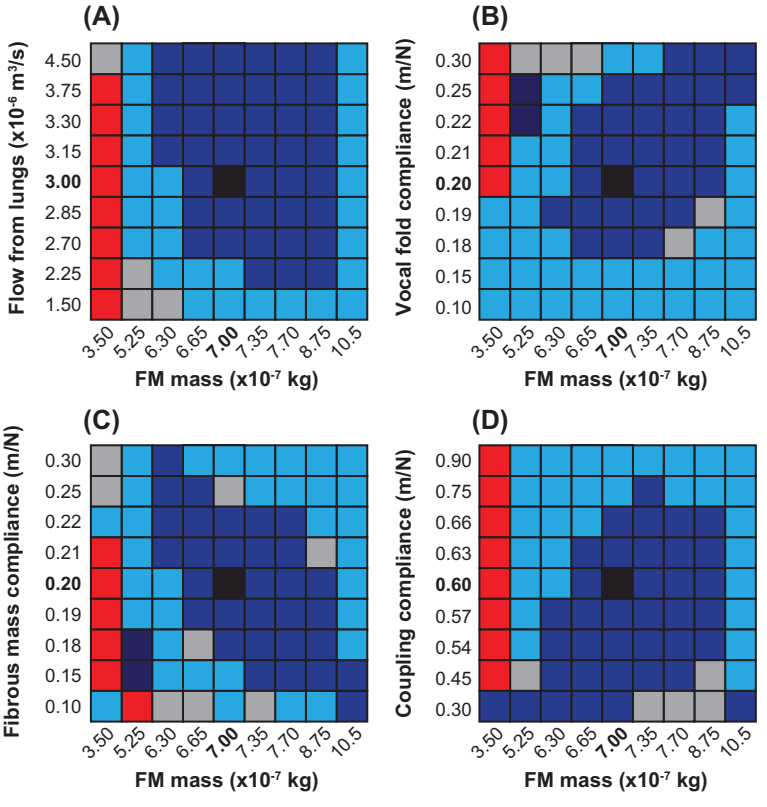

Figure 8. Parameter values that result in period doubling during simulations of the fibrous mass model. Plots show a combination of fibrous mass (FM) mass and (A) flow from the lungs, (B) fibrous mass compliance, (C) vocal cord compliance, (D) coupling compliance. In each, parameters vary from 50 to 150% of the values listed in Table 2; note that the scale is not linear. Light blue = sustained oscillations, Dark blue = sustained oscillations with period doubling, Grey = noisy or chaotic oscillations, Red = no sustained oscillations, Black = fibrous mass model parameters from Table 2.

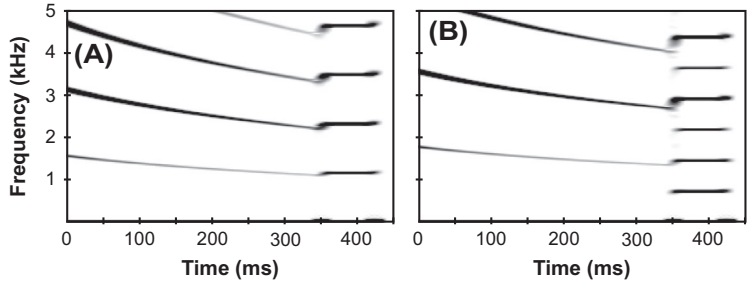

Figure 9. Spectrograms of flow through the vocal cord aperture in the 'whine-chuck' control (A) and fibrous mass (B) models. The entire simulated call is shown.

to the vocal cords of some taxa (Ryan and Drewes 1990; Boul and Ryan 2004; Gridi-Papp et al. 2006; Baugh et al. 2017). The bond graph models presented in this paper show that such a mass, when coupled to the vocal cords, can cause period doubling in vocal cord oscillation

that result in subharmonics. Period doubling in the vocal cords is not an inevitable outcome of the addition of a fibrous mass to the model, however, but depends on parameters that represent components of both vocal system morphology and behaviour.

Coupled oscillators are a common source of nonlinearities in animal vocal production (Wilden et al. 1998; Fitch et al. 2002; Beckers and ten Cate 2006; Suthers et al. 2011; Herbst et al. 2013). In our model, increasing pressure in the posterior laryngeal chamber causes displacement of the vocal cord. Air flows through the vocal cord aperture when the vocal cords are displaced, after which pressure decreases. Sustained oscillations in pressure, vocal cord displacement, and flow through the larynx persist when system parameters are appropriate (see also Kime et al. 2013). Pressure in the posterior larynx also causes displacement of the fibrous mass. Because pressure varies with the opening and closing of the vocal cords, the oscillation period of the fibrous mass is entrained to the oscillation of the vocal cords. A relatively large fibrous mass, however, may not complete a full cycle of oscillation with every vocal cord oscillation if its momentum is large. Impact oscillations, which occur when the fibrous mass collides with structures in the medial larynx and influence its momentum, are necessary for subharmonics in our model.

In túngara frog calls, a period doubling bifurcation occurs when flow from the lungs increases at the end of the whine for the chuck (Gridi-Papp et al. 2006; Bernal et al. 2009). Our models suggest that active (neural) modulation of the fibrous mass is not necessary for this transition between the spectral characteristics of the whine and chuck. We modelled the tissue connection between the fibrous mass and the vocal cords (Drewry et al. 1982; Guerra et al. 2014) as an elastic compliance. The restoring force of this compliance influences vocal cord displacement. Because the coupling restricts displacement of the vocal cords, the frequency of vocal cord oscillations shifts upward when a fibrous mass is included in the model. Period doubling in vocal cord displacement occurs when a large fibrous mass is entrained to the oscillation frequency of the vocal cords but has a different pattern of displacement such that the restoring force of the connecting compliance varies between vocal cord oscillations. A bifurcation to this behaviour may occur with changes in airflow and vocal cord compliance without active modulation of the fibrous mass itself.

Evidence from empirical studies with túngara frogs is consistent with the model presented here. The fibrous mass of adult males has thin (and thus possibly compliant) connections to both the arytenoid cartilages and the vocal cords (Guerra et al. 2014). Gridi-Papp et al. (2006) showed that, when the fibrous mass is ablated, chucks lack subharmonics. Ablation surgery also results in a decrease in whine frequency (Baugh et al. 2017), perhaps in part because the fibrous mass is unloaded from the vocal cord. Recent studies have also questioned the idea that frogs actively control the fibrous mass during chucks. Bernal et al. (2009) suggested that subharmonics in the túngara frog chuck are caused by impact oscillations of the fibrous mass. Subharmonics are sometimes present in the whines of túngara frogs, especially during periods of high air flow. This includes the beginning of the call, which often exhibits nonlinearities such as deterministic chaos and subharmonics (e.g. figures in Gridi-Papp et al. 2006). Likewise, subharmonics in the whine are present in males treated with arginine vasotocin who may have high rates of airflow through the larynx (Kime et al. 2010). Additional empirical studies that directly test the assumptions and dynamics of this model are necessary.

In other frogs as well, abrupt changes in the vibratory mode of the vocal cords occur with changes in airflow. As in our model, these shifts are due to passive changes in the dynamics of

oscillators within the system. The concave-eared torrent frog (*Odorrana tormota*) produces a myriad of complex call types with nonlinear properties (Feng et al. 2002, 2009; Narins et al. 2004). In experiments with excised larynges, Suthers et al. (2006) showed that nonlinear vocal complexity in these frogs can be explained by changes in airflow and sublaryngeal pressure. Similar experiments with excised larynges in treefrogs also showed evidence for nonlinearities in vocal cord dynamics (Gridi-Papp 2014).

Our model suggests targets of selection on the túngara frog vocal system, as well as possible constraints on the evolution of anuran vocal systems and communication signals. Ryan et al. (2010) suggest that preferences for lower frequency calls might have favoured the initial evolution of a fibrous mass that weights the vocal cords. Exaggeration of the fibrous mass and increasing separation from the vocal cords then might have resulted in the spectral characteristics of the chuck. Female túngara frogs prefer chucks produced with an intact fibrous mass (Baugh et al. 2017). In our model, the presence of a fibrous mass results in subharmonics characteristic of the chuck for many, but certainly not all, combinations of parameters. Our sensitivity analysis suggests that, indeed, subharmonics would be present in the chuck of a frog with relatively low compliance of the connection between the fibrous mass and the vocal cords, especially when the fibrous mass was small. Additional bond graph models could further explore evolutionary scenarios in which combinations of parameters (e.g. fibrous mass size, larynx size, tissue compliances, and flow from the lungs) evolved together.

Likewise, the ontogeny of the vocal system likely determines when chuck production is possible in juvenile frogs. The larynx, vocal cords and fibrous mass develop coincidentally in juvenile males, and stabilize prior to the size at which males begin to produce calls. Male túngara frogs initiate calling just after the development of the larynx is complete (Guerra et al. 2014). Again, additional bond graph models could explore switch points in ontogeny, when the relative size of vocal system components first allow for the production of whines, chucks, and the spectral characteristics of mature calls.

The lumped-element model presented here provides insight into the potential mechanisms by which an animal with a fairly simple vocal system might facultatively produce complex calls without extensive neural control of individual vocal system components. Rather than active control of the fibrous mass to produce the nonlinear characteristics of the chuck, it is possible that the vibratory mode of the fibrous mass and thus the vocal cords changes passively as a result of changes in airflow through the system. A wealth of studies has examined the selection pressures favouring the production of the chuck and the phylogenetic pattern by which the chuck arose. This study suggests the biomechanical changes that responded to selection favouring the chuck. Thus, we now know not only why the chuck evolved, but also how it might be produced.

Acknowledgements

We thank Monica Guerra for her insights into túngara frog larynx anatomy. We also thank two anonymous reviewers who provided helpful comments that improved the manuscript.

Disclosure statement

No potential conflict of interest was reported by the authors.

References

Akre K, Farris H, Lea A, Page R, Ryan M. 2011. Signal perception in frogs and bats and the evolution of mating signals. Science. 333:751–752.

Baugh AT, Gridi-Papp M, Ryan MJ. 2017. A laryngeal fibrous mass impacts the acoustics and attractiveness of a multicomponent call in túngara frogs (*Physalaemus pustulosus*). Bioacoustics. 4622:1–13.

Beckers GJL, ten Cate C. 2006. Nonlinear phenomena and song evolution in *Streptopelia* doves. Acta Zool Sin. 52:482–485.

Bernal XE, Page RA, Ryan MJ, Argo TF IV, Wilson PS. 2009. Acoustic radiation patterns of mating calls of the túngara frog (*Physalaemus pustulosus*): Implications for multiple receivers. J Acoust Soc Am. 126:2757–2767.

Breedveld PC. 2004. Port-based modeling of mechatronic systems. Math Comput Simul. 66:99–128.

Borutzky W. 2010. Bond graph methodology: development and analysis of multidisciplinary dynamic system models. London: Springer-Verlag.

Boul KE, Ryan MJ. 2004. Population variation of complex advertisement calls in *Physalaemus petersi* and comparative laryngeal morphology. Copeia. 2004:624–631.

Colafrancesco KC, Gridi-Papp M. 2016. Vocal sound production and acoustic communication in amphibians and reptiles. In: Suthers RA, Fitch WT, Fay RR, Popper AN, editors. Springer handbook of auditory research: vertebrate sound production and acoustic communication. New York (NY): Springer; p. 51–82.

Drewry GE, Heyer WR, Rand AS. 1982. A functional analysis of the complex call of the frog *Physalaemus pustulosus*. Copeia. 1982:636–645.

Dudley R, Rand AS. 1991. Sound production and vocal sac inflation in the túngara frog, *Physalaemus pustulosus* (Leptodactylidae). Copeia. 1991:460–470.

Feng AS, Narins PM, Xu CH. 2002. Vocal acrobatics in a Chinese frog, *Amolops tormotus*. Naturwissenschaften. 89:352–356.

Feng AS, Riede T, Arch VS, Yu Z, Xu ZM, Yu XJ, Shen JX. 2009. Diversity of the vocal signals of concave-eared torrent frogs (*Odorrana tormota*): evidence for individual signatures. Ethology. 115:1015–1028.

Fitch WT, Neubauer J, Herzel H. 2002. Calls out of chaos: the adaptive significance of nonlinear phenomena in mammalian vocal production. Anim Behav. 63:407–418.

Fletcher NH. 1992. Acoustic systems in biology. New York (NY): Oxford University Press.

Gans C. 1973. Sound production in the Salientia: mechanism and evolution of the emitter. Am Zool. 13:1179–1194.

Gerhardt HC, Huber F. 2002. Acoustic communication in insects and anurans: common problems and diverse solutions. Chicago (IL): University of Chicago Press.

Gridi-Papp M. 2003. Mechanism, behavior, and evolution of calling in four North American treefrogs [dissertation]. Austin (TX): University of Texas at Austin.

Gridi-Papp M. 2014. Is the frequency content of the calls in North American treefrogs limited by their larynges? Int J Evol Biol. 2014:11.

Gridi-Papp M, Rand AS, Ryan MJ. 2006. Complex call production in the túngara frog. Nature. 441:38.

Guerra MA, Ryan MJ, Cannatella DC. 2014. Ontogeny of sexual dimorphism in the larynx of the túngara frog, *Physalaemus pustulosus*. Copeia. 2014:123–129.

Herbst CT, Svec JG, Lohscheller J, Frey R, Gumpenberger M, Stoeger AS, Fitch WT. 2013. Complex vibratory patterns in an elephant larynx. J Exp Biol. 216:4054–4064.

Ishizaka K, Flanagan JL. 1972. Synthesis of voiced sounds from a two-mass model of the vocal cords. Bell Syst Tech J. 51:1233–1268.

Karnopp D, Margolis DL, Rosenberg RC. 2006. System dynamics: modeling and simulation of mechatronic systems. New York (NY): Wiley.

Kime NM, Ryan MJ, Wilson PS. 2013. A bond graph approach to modeling the anuran vocal production system. J Acoust Soc Am. 133:4133–4144.

Kime NM, Whitney TK, Rand AS, Ryan MJ, Marler CA. 2010. Treatment with arginine vasotocin alters mating calls and decreases call attractiveness in male túngara frogs. Gen Comp Endocrinol. 165:221–228.
Martin WF. 1971. Mechanics of sound production in toads of the genus *Bufo*: Passive elements. J Exp Zool. 176:273–293.
McClelland BE, Wilczynski W, Ryan MJ. 1996. Correlations between call characteristics and morphology in male cricket frogs (*Acris crepitans*). J Exp Biol. 199:1907–1919.
Narins PM, Feng AS, Lin W, Schnitzler H-U, Denzinger A, Suthers RA, Xu C. 2004. Old World frog and bird vocalizations contain prominent ultrasonic harmonics. J Acoust Soc Am. 115:910–913.
Pauly GB, Bernal XE, Rand AS, Ryan MJ. 2006. The vocal sac increases call rate in the túngara frog *Physalaemus pustulosus*. Physiol Biochem Zool. 79:708–719.
Rand AS, Ryan MJ. 1981. The adaptive significance of a complex vocal repertoire in a neotropical frog. Z Tierpsychol. 57:209–214.
Riede T, Tokuda IT, Farmer CG. 2011. Subglottal pressure and fundamental frequency control in contact calls of juvenile *Alligator mississippiensis*. J Exp Biol. 214:3082–3095.
Ryan MJ. 1980. Female mate choice in a neotropical frog. Science. 209:523–525.
Ryan MJ. 1985. The túngara frog: a study in sexual selection and communication. Chicago (IL): University of Chicago Press.
Ryan MJ, Bernal XE, Rand AS. 2010. Female mate choice and the potential for ornament evolution in túngara frogs *Physalaemus pustulosus*. Curr Zool. 56:343–357.
Ryan MJ, Drewes RC. 1990. Vocal morphology of the *Physalaemus pustulosus* species group (Leptodactylidae): morphological response to sexual selection for complex calls. Biol J Linn Soc. 40:37–52.
Schmidt RS. 1965. Larynx control and call production in frogs. Copeia. 1965:143–147.
Story BH, Titze IR. 1995. Voice simulation with a body-cover model of the vocal folds. J Acoust Soc Am. 97:1249–1260.
Suthers RA, Narins PM, Lin W-Y, Schnitzler H-U, Denzinger A, Xu C-H, Feng AS. 2006. Voices of the dead: complex nonlinear vocal signals from the larynx of an ultrasonic frog. J Exp Biol. 209:4984–4993.
Suthers RA, Wild JM, Kaplan G. 2011. Mechanisms of song production in the Australian magpie. J Comp Physiol A Neuroethol Sensory Neural Behav Physiol. 197:45–59.
Wells KD. 2007. The ecology and behavior of amphibians. Chicago (IL): University of Chicago Press.
Wilczynski W, Rand AS, Ryan MJ. 1995. The processing of spectral cues by the call analysis system of the túngara frog, *Physalaemus pustulosus*. Anim Behav. 49:911–929.
Wilczynski W, Ryan MJ. 2010. The behavioral neuroscience of anuran social signal processing. Curr Opin Neurobiol. 20:754–763.
Wilden I, Herzel H, Peters G, Tembrock G. 1998. Subharmonics, biphonation, and deterministic chaos in mammal vocalization. Bioacoustics. 9:171–196.